How to extract the critical size of clusters from AKMC simulations of precipitation

Joel Lepinoux

How to extract the critical size of clusters from AKMC simulations of precipitation

J. Lépinoux

ARTICLE HISTORY
Compiled 18th July 2022

Univ. Grenoble Alpes, CNRS, Grenoble INP, SIMaP, F-38000 Grenoble, France

Corresponding author: joel.lepinoux@grenoble-inp.fr

Abstract
The critical size of clusters is a well-known key quantity for precipitation modelling, especially for nucleation. Classically, its value is obtained from a mean-field model which approximates the free energy of clusters. AKMC simulations rely on a set of physical parameters defined at the microscopic scale, thus the nature of hypotheses is very different from its equivalent in phenomenological models. It has been shown recently than the free energy of clusters as well as other important quantities can be directly extracted from AKMC simulations. Thanks to these advances, the critical size for nucleation can now be derived from such measurements. In practice, one faces various problems depending on the quality of the available information. Thus, one has to adapt the measuring method to the different ranges of cluster size and/or the different stages of precipitation. This paper focuses on three methods, considering the precipitation in concentrated AlLi alloys as a model case to explore the evolution of the critical size versus the physical time, from nucleation to coarsening.

Keywords: precipitation, computer simulation, clusters, Monte Carlo, critical size, nucleation

1. Introduction

To manage nucleation, phenomenological models like the well-known KWN framework [1] rely on the Classical Nucleation Theory (CNT): it provides the critical size for nucleation and the steady-state nucleation flux (i.e. the number of supercritical clusters formed per unit time), a fundamental quantity for this type of model.

1.1. The critical size

According to the CNT, the change in free energy associated with the formation of a precipitate of size n (i.e., containing n solute atoms) in a binary alloy, writes:

$$\Delta G_n = V_n \Delta G_n^v + S_n \gamma \tag{1}$$

where $V_n$and S_n are respectively the volume and the surface of clusters of size n, in average [2]. The interfacial energy γ is assumed to depend only on temperature. In dilute and weakly supersaturated alloys, the driving force for precipitation per unit volume ΔG_n^v can be described by a simple approximation, e.g., the regular solution, especially if one considers pure segregation. Assuming spherical clusters of radius R_n, Equation (1) can be written:

$$\Delta G_n = (4\pi/3) R_n^3 \Delta G_n^v + 4\pi R_n^2 \gamma \tag{2}$$

Then, the critical radius is readily obtained:

$$R_n^* = \left(\frac{-2\gamma}{\Delta G_n^v} \right) \tag{3}$$

Ordered alloys, like the $L1_2$ structure considered in this work, are more requiring. More sophisticated models, e.g. the Cluster Variational Method, have to be used to produce results which can compare with atomistic simulations [3]. To get accurate results for small size clusters or to explore concentrations beyond high dilutions, the best way is to evaluate the partition function of clusters as a function of their size, for a given temperature. For very small clusters, this can be done directly; then, the number of states increases so quickly with the cluster size that methods from Statistical Physics have to be invoked [4]. Note that this kind of limitation is not restricted to solids, for instance, it concerns also the formation of water droplets [5].

The free energy of cubic clusters was calculated for the first time by Perini et al. in 1984 [6] using the overlapping distribution method proposed by Bennet (1976) [7]. This pioneering work showed that the free energy of clusters can be correctly described by a polynomial function which includes a volume term and a surface term, as in the capillary approximation (1-2), but requires also a term of line, i.e. in $n^{1/3}$, and a constant. This powerful method can provide accurate results but suffers of an important limitation: clusters are considered as finite systems, thus solute dilution has to be large enough to neglect interactions between close clusters.

1.2. The steady-state nucleation flux

Predicting the value of the steady-state nucleation flux is of course of the highest interest for modelling, as long as the number of supercritical clusters increases linearly with time. As soon as a deviation from linearity appears, the interest of this concept vanishes. Such deviations occur in concentrated alloys mostly because the solute concentration in the matrix is no more constant during nucleation.

Previous comparisons with AKMC simulations suggest a concentration threshold of the order of 1% at., for both pure segregation and ordered precipitates [2]. Of course, it is likely to depend on conditions, but the important point to understand is that the CNT framework is not appropriate to describe nucleation in concentrated alloys, whatever the quality of the model used to evaluate the precipitation driving force. Thus, to explore precipitation in concentrated alloys, one has adopt a more general point of view and to use more flexible tools. A good way to facilitate this process is to consider alloys of concentrations much larger than 1% at., as done in this work and previous ones.

1.3. An alternative bridge between atomistic simulations and precipitation models

In the literature, the critical size is considered as a key quantity (e.g., more than 500 occurrences of "nucleus" in [8]), but unfortunately, there is no experimental technique likely to provide direct measurements of the critical radius. If the concentration of clusters can be experimentally measured in some very dilute systems (see [9] for various examples), the critical size is always derived from the CNT and the capillary approximation described above. To our knowledge, it has never been extracted from atomistic simulations neither, even in such works the CNT is applied (e.g. [10]).

The main goal of this paper is to show how the critical size can be extracted from AKMC simulations. Generally speaking, the unbeatable advantage of numerical simulations is that the material properties can be fully controlled. In addition, one does not have to worry about impurities or structural defects likely to induce heterogeneous nucleation which can bias the results, etc. And most of all, the coordinates of all solute atoms are immediately available, which makes possible a number of analyses impossible to perform from experimental data.

Of course, we still need to translate the raw data provided by these simulations into some well-known quantities. Since the beginning of this work, we have chosen the framework of Cluster Dynamics (CD) for this purpose [11]. CD is a close relative of the CNT, then this formalism is fairly familiar to communities using the CNT. Furthermore, these two approaches are equivalent for dilute alloys [12]. One advantage of CD is that it can be used to describe all stages of precipitation with the same equations and coefficients, whose content can be easily enhanced with help of KMC simulations. Here

we recall the classical framework of CD. The evolution of C_n, the concentration of clusters of size n, is given by:

$$\dot{C}_n = (\alpha_{n+1}C_{n+1} + \beta_{n-1}C_{n-1}) - (\alpha_n + \beta_n)\,C_n \tag{4}$$

for $n>1$; for $n=1$ one can use the conservation of solute. Thus one has to solve a system of coupled differential equations.

The kinetic term β_n is the absorption coefficient, which is related to the diffusion coefficient D, the cluster radius and the monomer concentration; l is the lattice parameter:

$$\beta_n = 4\pi D R_n C_1 / l^3 \tag{5}$$

At first sight this expression is identical to that used in the CNT, but there are some subtle differences about the meaning of D and the concentration term (for a discussion see [2] and [12]). Again, Equation 5 is the classical expression for dilute alloys. A preliminary work have shown that in the general case, instead of C_1, one should use C_{ss}, the solute concentration in the solid solution [13] (this point will be revisited in a future work). In very dilute alloys, the solid solution is mostly composed of monomers, therefore all definitions converge. This is a typical example of findings which can be derived only from the study of concentrated alloys.

Then, the thermodynamics is introduced through the ratio of absorption and emission coefficients, β_n and α_{n+1}respectively :

$$\left(\frac{\beta_n}{\alpha_{n+1}}\right) = C_1 \exp\left(-\frac{F_{n+1} - F_n - F_1}{k_B T}\right) \tag{6}$$

with $k_B$the Boltzmann constant and T the temperature. Strictly speaking, this equation is convenient only for dilute alloys. With concentrated alloys, to get cluster distributions which compare well with those obtained by AKMC simulations, the above statistical calculation of F_n needs at least to be completed with an additional term of cluster gas entropy [14]. But recent studies have shown that this entropy correction is not fully correct and might become a source of error. This confirms that trying to enhance these classical frameworks (developed primarily for dilute alloys) with some corrective patches is not the right way. For instance, the assumption of isolated clusters required in the original statistical calculation of F_n is no longer valid in concentrated alloys. Indeed, these calculations must account for real conditions, i.e. the risk of coagulation between close clusters (i.e. when at least one solute atom become a bridge between two clusters), a risk which in addition evolves with time during precipitation. This is the critical point at the origin of a necessary change of approach. The successive steps of this evolution have been recalled and discussed in a recent work [15].

In the current formalism, we note F_n^* the free energy of n-mers accounting for the risk of coagulation between the considered cluster and its neighbours when it captures a new solute atom. To simplify, say that the calculation of F_n^* is similar to that of F_n, but includes an additional condition which accounts for the probability of coagulation. The principles of this calculation are detailed in [16]. Contrary to F_n in dilute alloys, we could not find any safe way to predict F_n^* without the help of AKMC simulations. Thus, the proposed strategy consists to rely on AKMC simulations up to the very beginning of nucleation, and then to approximate the evolution of F_n^* between this starting point and the final state at infinite time (obtained from the study of the system at the solubility limit).

Another consequence of this upgrade of CD formalism is the explicit introduction of the chemical potential of monomers, as explained in [17]:

$$\mu_1 = h_1 + k_B T \ln\left(\frac{C_1}{M_1}\right) \tag{7}$$

with $h_1$the monomer enthalpy. M_1 is the concentration of pure matrix sites: a pure matrix site is a matrix site whose all neighbours (its definition depends on the considered structure) are also matrix

sites. Flipping the occupancy of such a site into solute gives a monomer, and vice and versa. The concentration of pure matrix sites can be readily measured in simulations boxes [14, 15] and can be smaller than 0.1 in the present cases, while it is implicitly taken equal to 1 in classical models. In practice, managing μ_1 means modelling the evolution of M_1in the absence of the direct space (CD considers only the space of cluster sizes). Two complementary approaches can be used for this purpose, as discussed in [15]. Finally, in the new CD framework, Equation 6 writes:

$$\left(\frac{\beta_n}{\alpha_{n+1}}\right) = \left(\frac{C_1}{M_1}\right)\left(\frac{P^*_{n\to n+1}}{P^*_{n+1\to n}}\right) \tag{8}$$

where $P^*_{n\to n+1}$ and $P^*_{n+1\to n}$ are respectively the capture and release coefficients. Only the ratio $\left(P^*_{n\to n+1}/P^*_{n+1\to n}\right)$ is required, and it is a quantity which can be directly extracted from the analysis of clusters built in AKMC simulations [16]. This ratio is related to free energy F^*_n by:

$$\left(\frac{P^*_{n\to n+1}}{P^*_{n+1\to n}}\right) = \exp\left(\frac{h_1}{k_BT}\right)\exp\left(-\frac{F^*_{n+1}-F^*_n}{k_BT}\right) \tag{9}$$

In dilute alloys, equations 6 and 8 are equivalent, i.e. M_1=1, $h_1 = F_1$ and F^*_n=F_n. In other words, this new CD formalism has been made independent of solute concentration; usual expressions are only simplifications for dilute alloys.

Of course, the concept of critical size is unchanged: on average, clusters larger than the critical size are assumed to grow while those smaller than the critical size are assumed to dissolve.

2. AKMC simulations

Ordered and coherent $L1_2$ δ' Al_3Li clusters in aluminium are taken as a model case of concentrated binary alloy, and the data to analyse have been obtained by AKMC simulations. Fundamentals of this atomistic simulation technique can be found in [10] and the interatomic potential limited to first and second nearest neighbours (NN1 and NN2, respectively) used for this alloy has been described in [16]. As in previous works, four cases will be investigated here (NB: we consider only atomic concentrations):

(1) T=85°C and C_0=4.75%, moderate concentration and moderate excess of solute (+2.05%)
(2) T=200°C and C_0=8.25%, high concentration and moderate excess of solute (+1.95%)
(3) T=200°C and C_0=10%, high concentration and high excess of solute (+3.7%)
(4) T=85°C and C_0=9%, high concentration and very high excess of solute (+6.3%)

The interest of this selection is that the two cases of moderate supersaturation exhibit the expected stages of nucleation, growth and coarsening, while these stages seem to superimpose in the two other cases. AKMC simulations have been performed using simulation boxes of $[500]^3$ atoms (cases 1 to 3) or $[200]^3$ (case 4) to save computing time. Periodic boundaries conditions were applied. In case (4) we have also performed a simulation using $[500]^3$ atoms, until the excess of chemical potential of monomers reduces to 10% of its initial value. Both simulation box sizes lead to the same values of n^*, but of course, the measurements are much easier and accurate with a large box. All runs have been launched from a completely disordered state (random distribution of solute atoms). One of the great interest of such atomistic simulations is that the occupancy of any atomic site can be known at any time.

Thanks to these data, it has been shown recently that the free energy of clusters F^*_n evolves during precipitation as a function of the chemical potential of monomers [18]. The simplicity of this law is of high interest for modelling precipitation in concentrated alloys. Similarly, it has been shown that the ratio of cluster volume vs. their size evolves during precipitation, and as the evolution of F^*_n, this ratio can be easily modelled [19].

3. From AKMC simulations to Cluster Dynamics

In this section we introduce three methods to evaluate n^*, each one being particularly well-adapted to nucleation, growth or coarsening, respectively:

i) small size clusters, i.e., up to a few hundreds of solute atoms, which corresponds typically to the nucleation stage

ii) medium size clusters, i.e., from at least one hundred of solute atoms up to the end of the growth stage. For the situations investigated in this work this corresponds to clusters of a few thousands of solute atoms.

iii) large size clusters, which corresponds to the coarsening stage

However, there is no well-defined boundary between the application range of each method.

3.1. Small size clusters (method S)

Although the concept of critical size is widely used in the literature, its practical definition is customised following the referred framework; indeed, it has to be adapted to the available information. Our definition does not make exception to this rule: it is derived from the formalism of CD, the most convenient one to take advantage of data that can be easily extracted from AKMC simulations. In agreement with Clouet [2], we consider that a cluster of critical size has equal probabilities of capturing or releasing a solute atom. Thus, $n^*$is the value of n which satisfies $\alpha_n = \beta_n$. Knowing that β_n is proportional to the cluster radius R_n(cf. Equation 5), Equations 8 can be rewritten:

$$\left(\frac{P^*_{n-1\rightarrow n}}{P^*_{n\rightarrow n-1}}\right) = \left(\frac{M_1}{C_1}\right)\left(\frac{R_{n-1}}{R_n}\right) = \left(\frac{M_1}{C_1}\right)\left(\frac{N_{n-1}}{N_n}\right)^{1/3} \tag{10}$$

where N_n is the total number of sites attached to a cluster containing n solute atoms, in average. The ratio (R_n/R_{n-1}) is of course very close to 1, except for small clusters. First, one has to measure the average exclusion volume as a function of cluster size, then one assumes spherical clusters. The exclusion volume contains all sites connected to the solute skeleton of the cluster, by at least one NN1 bond or one NN2 bond, as detailed in [19]. Then, to obtain the radius to be used in Equation (10), some further modelling is required. Indeed, the interface shell of the exclusion volume can be shared among several clusters. Thus, the exclusion volume overestimates the effective volume of clusters. To account for this feature, it has been proposed to define a core volume [15]. The number of sites attached to the core volume N_{core} can be derived from the number of sites contained into the exclusion volume N_{ex} as follows:

$$N_{core}(n) = \left(N_{ex}^{1/3}(n) - \varphi\right)^3 \tag{11}$$

or

$$R_{core} = R_{ex}(n) - \varepsilon l \tag{12}$$

where $\varphi = 0.614$ and ε =0.24 (l is the lattice parameter). Note that for the cases investigated here, the relative difference between the two solutions for the ratio (R_n/R_{n-1}) is about 1% for n=5 and only 0.1% for n=20. Thus, this correction has negligible consequences on the calculated value of the critical size; nevertheless, it is useful for other purposes.

To derive reliable values of n^* from Equation (10), we have combined two strategies. A first method consists in fitting the difference between the *rhs* and the *lhs* terms in Equation (10). To fit the ratio $P^*_{n\rightarrow n+1}$, $P^*_{n+1\rightarrow n}$ we use the polynomial expression of F_n proposed by Perini et al. [6]:

$$F_n = \left(d\ln(n) + cn^{1/3} + bn^{2/3} + a\right) \tag{13}$$

All the quantities entering in Equation (10) fluctuate, which is likely to induce unexpected deviations of the estimated value of n^*, depending on the learning range chosen for the fit. The comparison of cluster distributions taken at various times from part to part from the considered one is an excellent way to detect artefacts and to correct them.

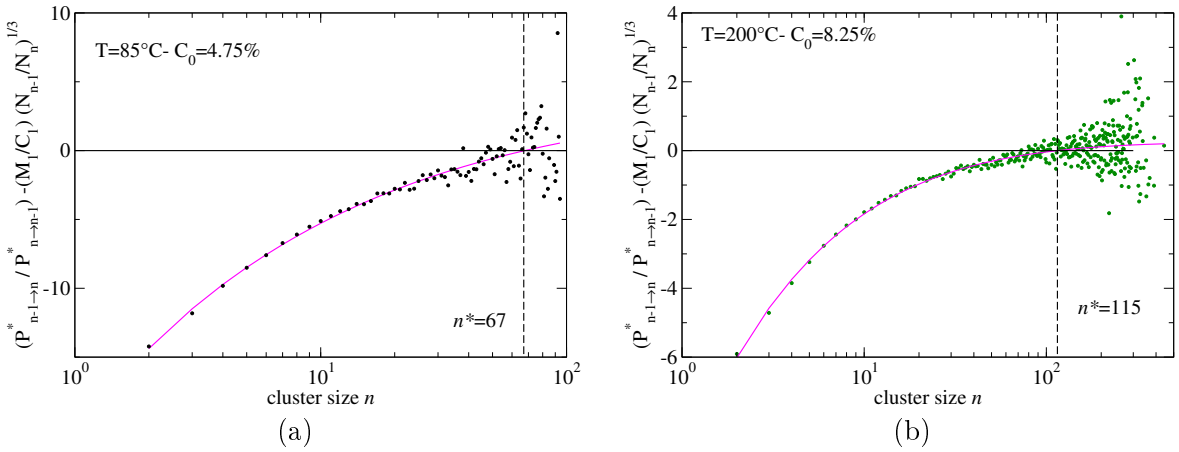

Figure 1.: Examples of application of method S1. (a) when n^* is very close to the size of the largest cluster (b) when the cluster distribution extends approximately up to $4n^*$.

Figure 1 shows two typical examples of this method S1. Figure 1a corresponds to the beginning of the first plateau of the nucleation stage in case (1) (cf. Section 3.2). There are only a few tens supercritical clusters, but the slope of the curve is high enough to provide an accurate estimation of n^*. The comparison with other results taken at various times taken within this plateau is very helpful to check the consistency of each result and to decide when this plateau starts and finishes exactly. Figure 1b is related to a distribution taken after the unique plateau of the nucleation stage in case (2). Here, the number of supercritical clusters is fairly high, and the results exhibit a wide dispersion. Note that the slope of this curve is much smaller than in the previous case, which makes more difficult the estimation of n^*. This situation is about the limit of what can be safely done with this method.

Another way to solve Equation (10) consists in fitting separately each member; then, the critical size is given by the intersection of the two respective fits. This method S2 is certainly the safest one; in addition, it can take advantage of already known fits of $P^*_{n\to n+1}$, $P^*_{n+1\to n}$ and (R_n/R_{n-1}), which are necessary for other purposes (see [15, 16]). Note that in this case, the ratio (M_1/C_1) should also be fitted to minimise the risk of artificial fluctuations. The main drawback of this method is that one cannot easily compare the fits of several close cases as previously to correct the inconsistencies that might be induced by some fluctuations.

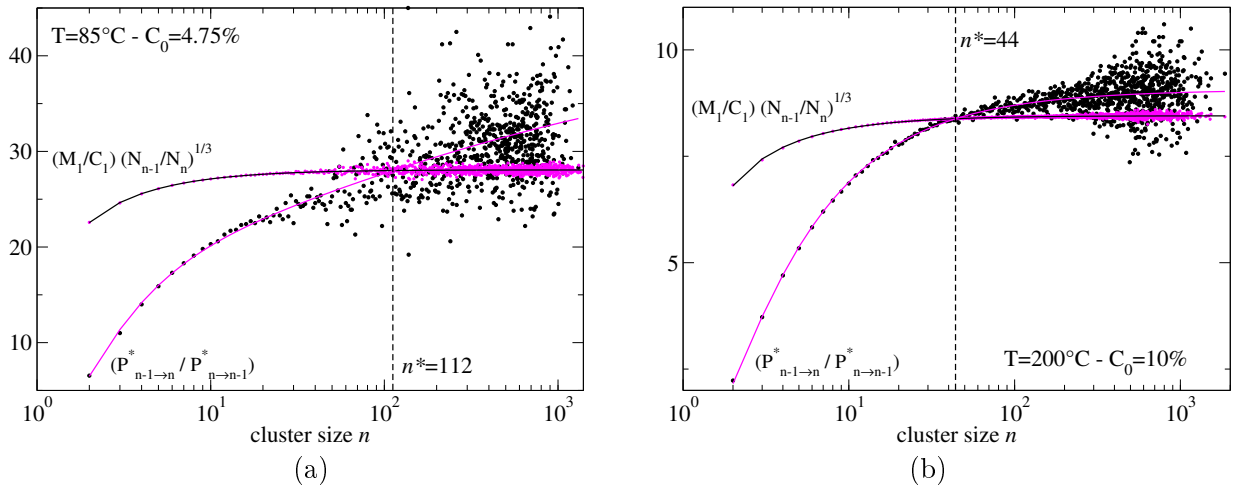

Figure 2.: examples of application of method S2. (a) n^* is ten times smaller than the size of the largest cluster (b) n^* is even smaller while the number of supercritical clusters is even larger. The two curves refer to the *lhs* and *rhs* terms in Equation (10).

Figure 2 shows two examples for which the method S1 fails. Fitting the *rhs* term in Equation (10)

is straightforward and provides accurate results which converge quickly toward the ratio (M_1/C_1). In case (a), for some reasons, the method S1 leads to a poor fit, while the method S2 gives a result fully consistent with others. In case (b), the fit obtained with the method S1 is apparently correct, but it leads to n^*=30 instead of n^*=44 with the method S2, again fully consistent with other results. This shows that even when the fit seems correct with the method S1, it has to be considered with caution. Thus, in practice, it is advised to use both methods to get the best of each one and to minimise the risk of error.

Note that Equation (10) refers to pairs of contiguous classes of cluster sizes n and (n-1). Thus, the cluster distribution is assumed to be continuous, ideally at least up to a few ten classes beyond n^*. And ideally, the last classes in this range should contain at least a few clusters. These two conditions are always satisfied at the beginning of precipitation kinetics in the four cases investigated here, thus Equation (10) is very suitable for the calculation of n^*, at least in the nucleation stage. Then, when the cluster distribution extends, the information gets poorer and poorer between the range of size which corresponds to the solid solution and that of supercritical clusters. Similarly, the distribution tail provides very scarce information. This means that the solution S has to be used with great care when n^* exceeds typically one or two hundred atoms.

3.2. Medium size clusters (method M)

As explained in the previous section, due to the decreasing quality of the method S (variant 1 or 2) when n^* is larger than a few hundreds, an alternative method should be adopted. By analogy with Equation (5), we start from the following approximation:

$$\left(\frac{\beta_n}{\alpha_n}\right) \approx \left(\frac{C_1}{M_1}\right)\left(\frac{P^*_{n\to n+1}}{P^*_{n\to n-1}}\right) \tag{14}$$

Of course, it is not designed to provide a good agreement for very small clusters, but by construction, this solution should converge towards the previous one, even at intermediate sizes. To estimate the error, Figure 3 compares the evolution of the second members in Equations (10) and (14). Indeed, to be exact, Equation (14) should verify:

$$\left(\frac{P^*_{n\to n+1}}{R_n}\right) / \left(\frac{P^*_{n-1\to n}}{R_{n-1}}\right) - 1 = 0 \tag{15}$$

Figure 3 reports this quantity for two different cases:
- T=85°C, C_0=4,75%. For this very classical case, a regular decreasing is observed.
- T=200°C,C_0=10%. This case has been chosen because it exhibits a non-conventional behaviour as described in [15]. It is characterised by the formation of a percolating phase of connected clusters during the growth stage, which subsequently dissociate to give a classical cluster distribution during coarsening. As can be seen, even in a such non-conventional situation, this method provides an excellent approximation provided its use is restricted to clusters larger than typically a few hundreds. For the situations explored here, this amounts to exclude the nucleation stage.

As can be seen in Figure 4, the method M can use data for supercritical clusters which are much denser and less dispersed than those available for method S, which is more efficient for small clusters. Thus, this solution M provides a better account of medium and large clusters as soon as n^* is of the order of a few hundreds. In some cases, this method fails to provide an acceptable description of small clusters, which is not surprising, but might bias the fit. In such cases, it is possible to combine the two solutions S and M to take advantage of the best description of small clusters with Equation (10) and medium to large clusters with Equation (14).

3.3 Large size clusters (method L)

As for the transition from method S to method M, strictly speaking, the validity of Equation (14) is not limited by the large size of precipitates. However, when n^* increases, the slope of the curves

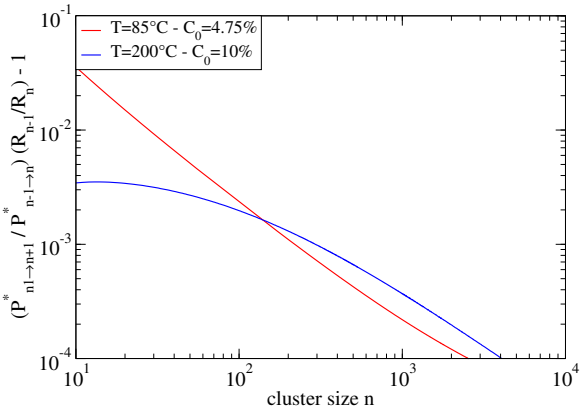

Figure 3.: testing the validity of Equation (14).

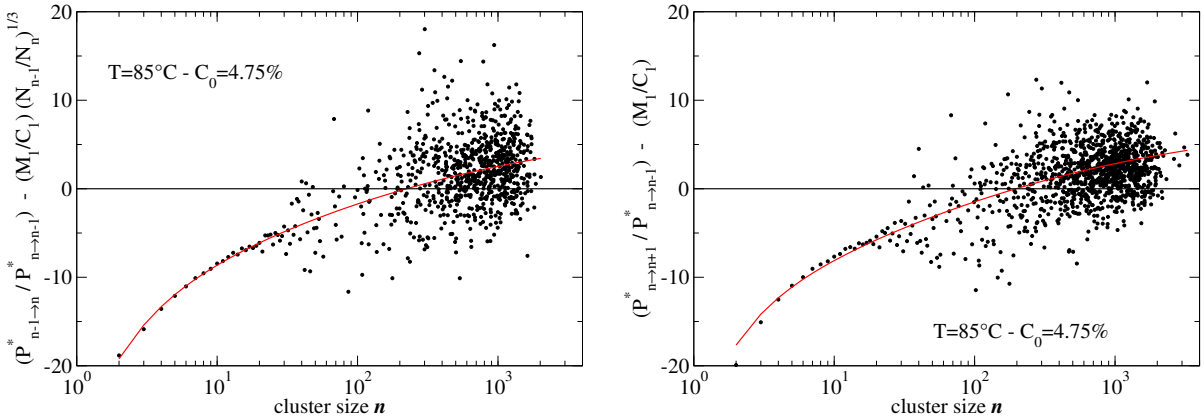

Figure 4.: a comparison of methods S (a) and M (b) for n^*=210±10. With such a value of n^* the method M (equation (14)) is fairly easy while the method S (equation (10)) is rather difficult.

reported in Figures 2 and 3 decreases aroundn^* and this induces a fast-growing of the uncertainty of the calculated value (see Figure 5a). As previously, it is preferable to adopt another method which avoids this drawback.

From the analysis of AKMC data, it is possible to monitor the growth of individual clusters, using a sample of snapshots taken at regular time interval. Then it is easy to select a range of cluster size such that large clusters grow and small ones shrink. This selection can be subsequently refined to ease the search of n^*. Knowing that the size of clusters is a very fluctuating quantity, one has to consider a range of time (centred on the given time) large enough to capture a significant change of cluster size.Nevertheless, it should not be too large, to avoid a significant evolution of the whole system during this time. For instance, during such a typical time window, the relative change in the concentration of the solid solution can vary from a few percent near the transition between nucleation and growth to 0.1% at the beginning of the coarsening stage. These small differences do not justify to improve this method, which is elementary, compared with the two previous ones. Nevertheless, it is preferable to limit its use to the coarsening stage, although in some conditions it has been proved to give the same results as the two other methods around the end of the nucleation stage. After various trials, we chose to consider a set of 25 measurements taken at constant time step (figure 5b). Then, for each analysed cluster, the variation of size is fitted by a straight line and its slope is calculated: a horizontal line corresponds to n^* (in practice, a quadratic curve is often preferable). One could object that reporting R_n^2 versus time would be physically more justified than reporting N_n or R_n^3 versus time, but we have checked that this has no effect on the calculated value of n^*.

As can be seen in Figure 5a, the curve related to Equation (14) exhibits a tiny slope around n^* and the distribution of the information is very heterogeneous between the solid solution and precipitates. Consequently, the uncertainty is rather large: [890 – 1300] depending on the learning range used to fit simulation data. In figure 5b, despite that the evolution of cluster sizes is not monotonous, n^* can be

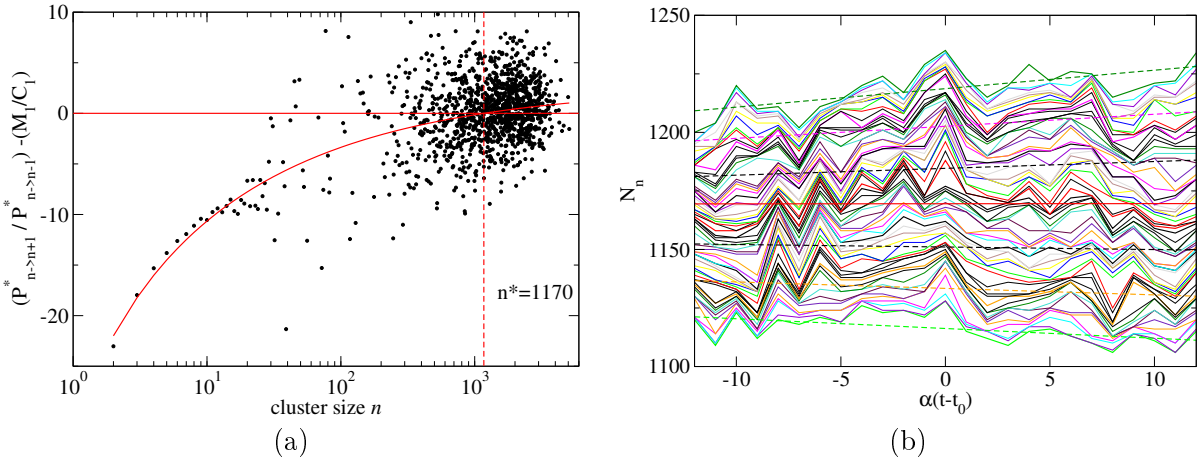

Figure 5.: comparison of methods M and L near the transition between the growth and the coarsening stages: in both cases, n^*=1170. (a) method M, n^* is given by the intersection of the curve and the X-axis; (b) method L, n^* is given by the straight line (i.e., fit) which minimises the absolute value of its slope (the horizontal red line). Each curve is related to a particular cluster. The bold straight lines are the fits associated to the bold curves of same colour.

calculated unambiguously and quickly. Occasionally, some event induces large variations of N_n, which makes it difficult or even impossible to decide. This is easily solved by translating the time window to avoid the perturbation. But in average, this measurement remains fairly easy and above all very fast because method L requires only cluster sizes, which can be readily obtained from simulations. In comparison, the two previous methods require heavy calculations before attempting to determine n^*. However, if the aim is to gather all data necessary to set up CD calculations, for instance, no additional data are required. Nevertheless, evaluating Equation (10) or (14) is not a trivial task, it takes a lot of time to check the consistency of results.

4. Results

4.1. General remarks

Starting from a random state (pseudo infinite temperature), whatever the target temperature and the supersaturation,n^*always starts from a virtually infinite value. Then, when imposing a finite and constant temperature, n^* decreases rapidly while the system evolves toward quasi-equilibrium (see [17] about this notion). Then, n^*reaches a minimum n_0^* before increasing.

The lower the super-saturation, the lower the fraction of super-critical clusters when n^*reaches its minimum n_0^*. In very dilute alloys, this fraction is null. And of course, on the contrary, the higher the supersaturation, the higher the fraction of super-critical clusters when n^*=n_0^*, a fraction which rapidly tends toward 1. Figures 6 (a-d) compares the evolution of n^*as a function of time for the four cases investigated here. In addition, for each case, we have also reported the evolution of $\Delta\overline{\mu}$, the associated excess of the chemical potential of monomers (cf. Equation (7)) normalised by k_BT, to better put into evidence the correlations between these two quantities.

$\Delta\overline{\mu}$ writes (see [17] for details):

$$\Delta\overline{\mu}(t) = \left(\frac{\mu_1}{k_BT}\right)(t) - \left(\frac{\mu_1}{k_BT}\right)(t \to \infty) \tag{16}$$

	(1) 85°C/4.75%	(2) 200°C/8.25%	(3) 200°C/10%	(4) 85°C/9%
Δt_{N_I}	12	2	1.3	1.8
$\Delta t_{G_{II}}$		19	245	890
Δt_{G_I}	17	36	17	
n_{nucl}	67-70	59	42	14
$\%N_I$	98	26	0	2
$\lambda_{G_{II}}$		0.12	0.59	0.64
λ_{G_I}	2.13	1.86	1.25	
$\delta\left[\Delta\overline{\mu}_{N_{II}}\right]$		0.69#	1.143#	1.377
$\delta\left[\Delta\overline{\mu}_{N_I}\right]$	0.025	0.025	0.02	0.1
$\delta\left[\Delta\overline{\mu}_{G_{II}}\right]$		0.0457	0.39	0.89
$\delta\left[\Delta\overline{\mu}_{G_I}\right]$	0.28	0.15	0.12	
$\delta[\Delta\overline{\mu}_C]$	0.155	0.09	0.05	0.16

Table 1.: main features of n^*(t). Δt_X: the ratio between the final time and the onset time of stage X. n_{nucl}: the critical size during the nucleation plateau. $\%N_I$: the relative contribution of the solid solution to nucleation (cf. Section 3.2). λ_X: the time exponent in the fit of stage X (0 for nucleation I and 1 for coarsening). $\delta[\Delta\overline{\mu}_X]$: the variation of $\Delta\overline{\mu}$ in stage X. In case (1) n_0^*=48, otherwise n_0^*=n_{nucl}. (#) At T=200°C, the minimum of $\Delta\overline{\mu}$ does not correspond to t=0, contrary to what is observed at T=85°C.

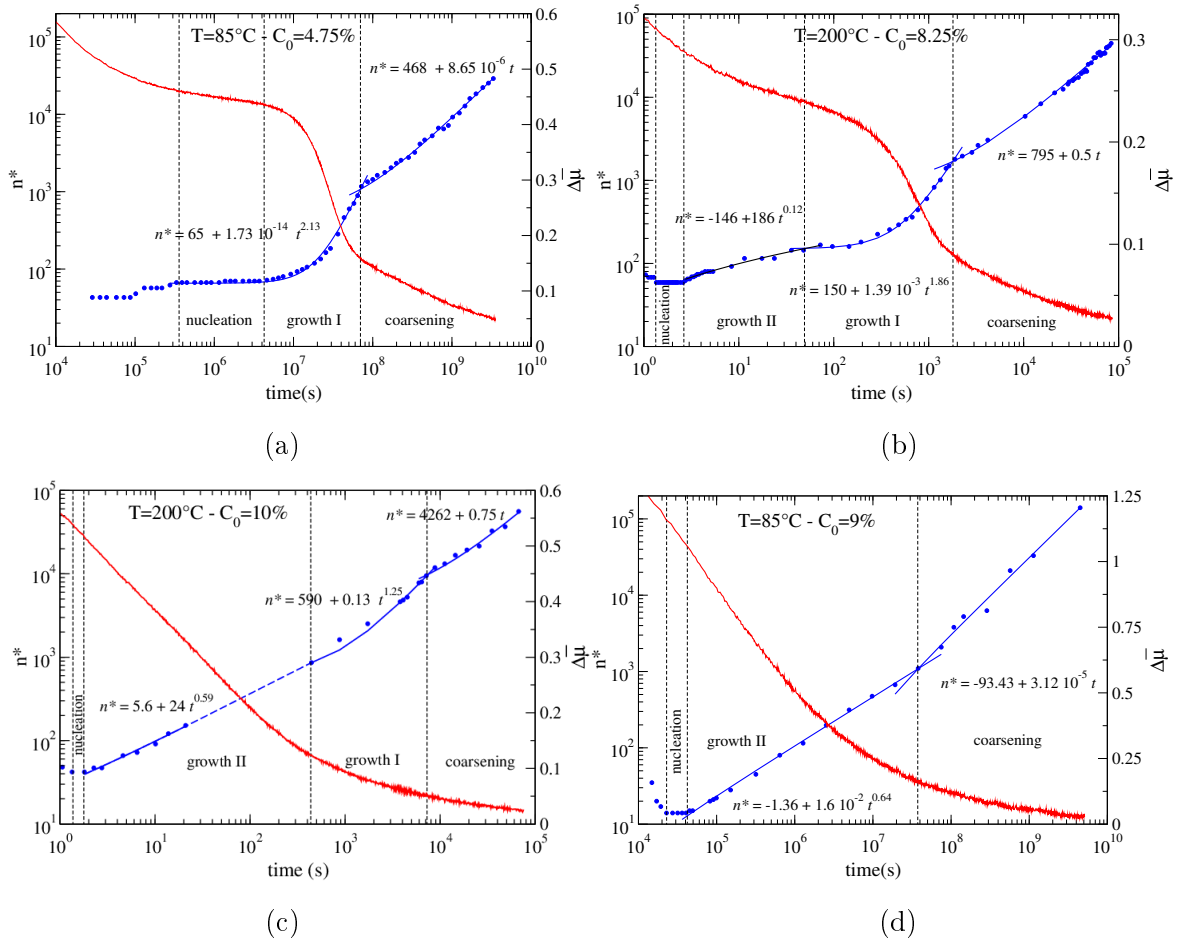

Figure 6.: main results for the four studied cases (cf. section 2). The symbols and their fit (blue online) and the left Y-axis are related to the critical size while the plain curves (red online) and the right Y-axis are related to the excess of chemical potential.

4.2. Analysis of case (1)

As expected from the evolution of its chemical potential (Figure 6a), n^* exhibits three distinct ranges, like the average size in dilute alloys:

- the nucleation stage is a long plateau (one decade on the time axis). In details, it is composed of two subsets (n^*=67 and n^*=70), but for a global description of n^*(t) it can be considered as a simple plateau.

- a classical growth stage (labelled 'growth I' in Figure 6a) associated with a fast increase of n^*, from 70 to about 1000.

- and finally, a coarsening stage associated to a clear slowdown of the increase of n^*.

The pre-nucleation stage was not called "incubation", because this notion related to the CNT does not appear relevant in this context. Indeed, a close examination of the concentration of supercritical clusters (to be presented in details elsewhere) reveals that nucleation really starts near the beginning of this plateau and that the maximum of supercritical clusters is reached at the end of this plateau. This plateau also corresponds to the beginning of the quasi-equilibrium state, which is another reason to disregard the details of this pre-nucleation stage. The initial cluster distribution is compact and n_0^*=43. This value is too close to the size of the largest clusters to safely define intermediate values of n^* (i.e., n^*>43), even with a simulation box of 500^3 atoms. Then, n^* increases slowly, exhibiting two steps of various length until it reaches the nucleation plateau.

To fit n^*(t) during the growth stage, we have used the trial function $n* = n_0 + \theta t^{\lambda}$. Including the nucleation stage in the fit was not intentional, but letting the exponent λ free produces a fit which describes both stages with a unique curve. Note that the exponent λ is slightly larger than 2.

In the coarsening stage, it is well-known that the distribution of precipitate sizes scaled by n^* converges toward a self-similar distribution, extensively discussed in the literature (see for instance [20, 21]), including in concentrated alloys [22]. Although there is no specific model predicting the evolution of the critical size from the transition with growth, we have assumed that its evolution can be described again by a power law, as the average size of precipitates. Thus, we have tried to impose λ=1. As can be seen in Figure 6a, this trial function works fine, including from the sharp transition with the growth stage (n^* is still smaller than the average size of precipitates).

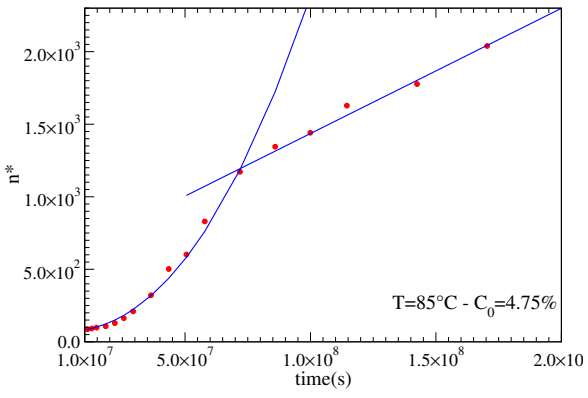

Figure 7.: zoom on the transition between growth and coarsening, taken from Figure 6a with linear scales for both axes.

Comparing the concentrations of supercritical clusters at the end ($C^{max}_{n>n^*}$) and at the beginning of the nucleation plateau ($C^{0}_{n>n^*}$) reveals that supercritical clusters present before the onset of nucleation contribute only for 2% to the formation of precipitates. In other words, despite a solute concentration of 4.75%, this case (1) is very close to the dilute alloy asymptote.

Note that $\Delta\overline{\mu}$ decreases first rapidly, then slows down before the nucleation stage, during which it is almost constant (from 0.46 to 0.435). Then, at the transition between growth and coarsening, $\Delta\overline{\mu}$

falls to 0.16, which is about one third of its value when $n^*=n_0^*$ (cf. Table 1).

For sake of consistency, the whole coarsening stage has been investigated using the method L, (cf. section 2). Note that the transition between growth and coarsening is very sharp, especially in cases 1 and 2 due to the large difference between the time exponents of these two regimes. Figure 7 focuses on this part of Figure 6a, using a linear scale for both time and n^*.

At first sight, this behaviour seems induced by the change of method, from M to L, but in fact the change of method occurs before the crossover of the respective fits of growth and coarsening regimes. Indeed, when approaching this crossover, method M deviates and never converges toward the fit given by method L for the coarsening regime. On the contrary, when applied to the end of the growth branch, from this cross-over, method L converges toward the fit of this regime given by method M. Thus, method L should be preferred to explore the end of the growth regime, instead of method M which becomes less and less reliable due to the impoverishment of data.

However, one should keep in mind that method L assumes that the whole cluster distribution evolves slowly, which is typically the case in the coarsening regime. Thus, the application of method L to the growth branch should be as limited as possible and at this stage, one cannot exclude an artefact. Much larger simulation boxes would be necessary to investigate this region in details. However, the sharpness of this transition is much less important than our ability to describe these two regimes with simple power laws.

Although we have used a fairly large simulation box, one should be aware that the largest average cluster size at the end of present simulations is only the half of the smallest experimental values reported in [23], for instance. This shows that the very long times are still unreachable for such simulations.

4.3. Analysis of case (2)

Comparing Figures 6a and 6b suggests that cases (1) and (2) are very similar. Their respective excess of solute are equivalent, about 2%, but their respective excess of chemical potential differ by a factor 2. Another major difference is the initial distribution of clusters, compact in case (1) and extended in case (2). Consequently, the initial decreasing of n^* before it reaches its minimum is easy to put into evidence, while it is almost impossible in case (1). In Figure 6b, only a few measurements have been reported before n^* reaches its minimum $n_0^*=59$. Again, the onset of nucleation corresponds to the beginning of the plateau $n^*=n_0^*$, but in this case, the number of super-critical clusters is already fairly large. Consequently, comparing $C_{n>n*}^{max}$ and $C_{n>n*}^{0}$ indicates that supercritical clusters present before the onset of nucleation contribute now for 74% to the formation of precipitates. There is still a classical nucleation stage, but its contribution is now minority.

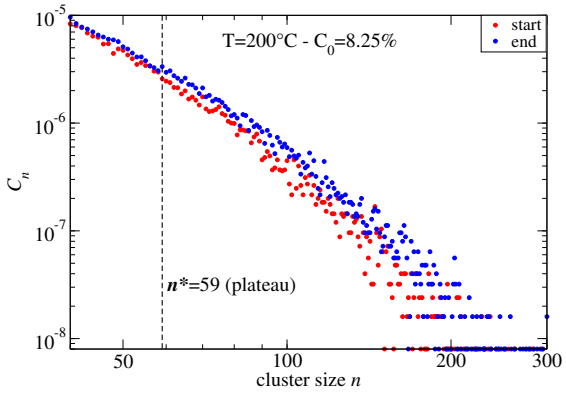

Figure 8.: comparison of cluster distributions at the beginning and the end of the first plateau in case (2).

This situation presents a special interest: it gives us an opportunity to validate our calculated value of n_0^*. Figure 8 compares the cluster distributions at the beginning and at the end of the nucleation plateau. While the first one is regular, the second one exhibits a clear shift at n^*=59, which is the value found for $n_0{}^*$. Unfortunately, for various reasons, such a comparison is not possible in other cases.

Before reaching a growth stage very similar to that observed in case (1), we have introduced a new stage, labelled "growth II" in Figure 6b. As in case (1), we have used a power law to describe this new growth stage. Note that as in case (1), the fit of the growth stage I includes the initial plateau, but the exponent λ is now slightly smaller than 2. In the growth stage II, λ takes a tiny value, close to that of the nucleation stage (null). We have defined the transition between the two growth stages by the crossing of their respective fits, as reported in Figure 6b.

The transition at the transition with the coarsening stage is not as sharp as in case (1), but again, imposing λ=1 provides a good fit for the coarsening stage, even at the transition. A consequence of the low contribution of the fluctuations of the solid solution is the correlation between the respective evolutions of n^* and $\Delta\overline{\mu}$ which is not as clear as in case (1). However, note that at the transition between growth and coarsening, $\Delta\overline{\mu}$ is again about one third of its value when n^*=n_0^*. Its total variation is only half of its equivalent in case (1) and the excess of solute is similar (about 2% in both cases). All these features are recalled in Table 1.

4.4. Analysis of case (3)

As can be seen in Figure 6c, the $\Delta\overline{\mu}$(t) curve no longer exhibits the characteristic shape observed in Figures 6a and 6b. It is as if the central part, related to growth, would have been flattened. As previously, n^* reaches a minimum, but now, it corresponds to a tiny plateau while the concentration of supercritical clusters is much larger than in case (2). Consequently, the contribution of the solid solution to the formation of precipitates is too small to be safely measured. Then, we have a long stage of growth II (cf. Table 1) before a short stage of growth I, without a clear transition contrary to case (2). However, the transition between the growth I stage and the coarsening stage is again well-defined. Note that, compared with case (2), the time exponent increases in the growth I stage while it seriously decreases in the next stage. Remark also that most of the decrease of $\Delta\overline{\mu}$ occurs in the growth I stage. The second part of this stage (i.e., the dashed line in Figure 6c), where no KMC data is reported, corresponds to the presence of a percolating phase extending over the whole system. This means that most clusters are connected to their neighbours. Therefore, our usual measurements are meaningless in this context. However, this does not have any consequence on the precipitation behaviour. For instance, note that the point lying at the interface between the two growth stages in Figure 6c is in excellent agreement with the fit of growth II. As reported in [15], this behaviour has been observed in case (4) too, but only with a small simulation box, while it vanishes with a large one. This suggests that in case (3), this behaviour would require a huge simulation box to disappear.

4.5. Analysis of case (4)

As can be seen in Figure 6d, in case (4), the $\Delta\overline{\mu}$(t) curve seems very similar to that of case (3). But the n^*(t) curve exhibits a major new feature: the growth I stage has been entirely replaced by the growth II stage. Note that its time exponent has increased, compared with the two previous cases. Again, the transition with the coarsening stage is well-marked and as in case (3), most of the decrease of $\Delta\overline{\mu}$ occurs before the onset of coarsening. Note that the total variation of $\Delta\overline{\mu}$ is twice larger than in cases (1) and (3). The nucleation plateau is long enough to evaluate the contribution of fluctuations of the solid solution to the formation of supercritical clusters: 2%, to be compared with the 98% of case (1).

This case (4) ends our presentation of the four scenarios encountered in this work, with a consistent evolution from case (1) toward case (4) (cf. Table 1).

5. Conclusion

5.1. About methods

To our knowledge, it is the first time that the critical size of clusters has been extracted from AKMC simulations. In this paper, we have presented three methods to evaluate n^*:

- the method S is the most convenient one for small clusters and/or the nucleation stage. It can be applied following two slightly different ways. Both have advantages and drawbacks. Using the most accurate one is not an option, but knowing that the measurements can be deprecated by various sources of bias, it is advised to check the consistency of results thanks to the other form. Indeed, as n^* is fairly small during nucleation, accuracy, and reliability of fits should be as high as possible:

- the method M is well-adapted to medium size clusters and to the growth stage. When possible, it should be compared with the other methods, especially near the transitions with nucleation and coarsening.

- the method L is the best one for large clusters and the coarsening stage. It is often interesting to extend its application beyond the transition with the growth stage.

The methods S and M are based on the calculation of a pair of parameters for each cluster size, using the 'CapRel' method described in [16]. In comparison, the method L is very light. Whatever the method, the evaluation of n^* is rarely an easy task; almost each cluster distribution is a new challenge which requires some choices. Only a careful examination of various solutions at various times allows selecting the most consistent one. The continuous evolution from scenario (1) to scenario (4) reported in Figure 6 strongly supports the reliability of our evaluations of n^*(cf. Table 1). In case (2), it has been possible to find an independent proof to confirm the accuracy of our estimation for n_0^* during nucleation (cf. Figure 8).

5.2. About results

As expected, the application of these methods provides various new insights that should be accounted for to reconsider our views about precipitation. By analogy with the evolution of the average size of precipitates, to describe n^*(t), we have defined several stages and proposed associated fits based on simple power laws.

The easiest stage to define is the last one, because its onset takes the form of a sharp transition with the previous stage. Running these simulations over a significant range of time beyond that point has allowed us to show that from the transition, n^*(t) is well-described by a simple power law whose time exponent equals to 1, like the classical law giving the evolution of the average size of precipitates.

Concerning growth, i.e., the stage preceding coarsening, we have shown that n^*(t) exhibits two forms of growth. The one noted 'growth I' is a stage of fast increasing, unambiguously related to the stage of fast decreasing of $\Delta\overline{\mu}$. Its time exponent, about 2 in cases (1-2), slightly decreases in case (3), and finally, this stage vanishes in case (4). From case (2), a new growth stage appears, noted 'growth II'. While increasing supersaturation, this stage extends at the expense of the classical growth stage and finally it is the only growth stage in case (4). Note that the time exponent increases, but remains lower than 1, the exponent of coarsening, contrary to the time exponent of growth I, which is always larger than 1 (note however that growth II is much faster than growth I).

By analogy with these two growth stages, one could also define two nucleation stages (not mentioned before to not overload Figure 6). As for growth, case (1) exhibits only the classical form of nucleation, i.e., a long plateau during which large fluctuations transform into precipitates: this is the classical picture. Another particularity of case (1) is that n_0^* is lower than n^* during the nucleation plateau (denoted n_{nucl}^* in Table 1), but apparently, this pre-nucleation stage does not play any significant role. In the three other cases, before the onset of the nucleation plateau, there is a stage of fast decreasing of n^*. And as n_0^* is much smaller than the maximum size of clusters, this could be considered as a secondary type of nucleation.

In the literature, these clusters are sometimes denoted 'pre-existing clusters' to indicate that they are already formed when n^* reaches its minimum value, contrary to those formed from fluctuations of the solid solution. Exactly as the growth II stage, unknown in case (1), this stage becomes dominant at higher supersaturation. In case (3), it is even the only form of 'nucleation', although there is a tiny plateau. Classical nucleation is still measurable in case (4) but it is negligible. During this stage,

supercritical clusters do undergo important transformations; thus this stage should not be confused with a purely mathematical construction. To summarise, the relative weight of form II of both nucleation and growth versus their form I, is mostly governed by the excess of solute.

As the different stages of $n^*(t)$ are well-defined, the notion of overlap of the different stages of the evolution of precipitates, as described by Robson [24], does not apply ton^*. However, these different stages are very similar to those observed on the curves $\Delta\overline{\mu}(t)$. And by analogy with the kinetic map proposed by Robson (cf. Figure 6 in [24]) one could define another map to put into evidence two domains, i.e., one related to cases (1-2) and the other one related to cases (3-4). However, instead of 'supersaturation' in abscissa we recommend the excess of solute; instead of γ, the free interface energy, in ordinates, we propose the solubility limit, a quantity which contains more information than γ (a criterion inherited from the CNT). With these changes, from the analysis of ten situations, the change of $\Delta\overline{\mu}(t)$ from type (1-2) to type (3-4) occurs along a line of almost constant excess of solute: from 2.55% at 250°C to 2.95% at 50°C. These two domains of $\Delta\overline{\mu}$ correspond to the two types of growth of n^*. This evaluation could be easily refined, but its interest for n^* is questionable owing to the complexity of the relation between $\Delta\overline{\mu}$ and n^*. It seems more interesting to explore how the behaviour of $n^*(t)$ controls that of the average size of precipitates, for instance.

More generally, the possibility to extract n^* from AKMC simulations, allows revisiting the phenomenological laws used to describe precipitation [25], while avoiding any reference to the CNT. In addition, it might be interesting to consider the application of these findings to dilute alloys.

Acknowledgements

Dr. E. Clouet is gratefully acknowledged for providing his AKMC package.

References

[1] R. Wagner and R. Kampmann, *Homogeneous second phase precipitation, in Materials Science and Technology*, Eds. R. W. Cahn, P. Haasen, and E. J. Kramer, Vol. .5, Chapt. 4, Verlag Chemie GmbH, Weinheim (1991) pp. 213 - 304.

[2] Clouet E 2010 Modeling of nucleation processes ASM Handbook, vol. 22A Fundamentals of Modelling for Metals Processing ed D U Furrer and S L Semiatin vol 22A (Material Park, OH: ASM International) pp 203–19

[3] A. Clouet, M. Nastar and C. Sigli, Nucleation of Al3Zr and Al3Sc in aluminium: from kinetic Monte Carlo simulations to classical theory, Phys Rev. B 69 (2004) pp. 064109-(1-14).

[4] Lépinoux J 2005 Interfacial reaction rates and free energy of cubic clusters *Phil. Mag.* **85** 3585–3621.

[5] Ford IJ 2004 Statistical mechanics of nucleation: A review Proceedings of the Institution of Mechanical Engineers, Part C *Journal of Mechanical Engineering Science* **218** 883-899

[6] Perini A, Jacucci G and Martin G 1984 Cluster free energy in the simple-cubic Ising model *Phys. Rev. B* **29** 2689–97

[7] Bennett C 1976 Efficient estimation of free energy differences from Monte Carlo data, *J. of Computational Physics* **22** 245-268.

[8] Kashiev D 2000 Nucleation: Basic Theory with Applications (Amsterdam: Elsevier)

[9] Kelton K F and Greer A L 2010 Nucleation in condensed matter: Applications in materials and biology (Oxford: Pergamon)

[10] Soisson F and Martin G 2000 Monte Carlo simulations of the decomposition of metastable solid solutions: transient and steady-state nucleation kinetics *Phys. Rev. B* **62** 203–14

[11] Clouet E, Barbu A, Laé L and Martin G 2005 Precipitation kinetics of Al_3Zr and Al_3Sc in aluminum alloys modeled with cluster dynamics *Acta Mater.* **53** 2313-2325

[12] Martin G 2006 Reconciling the Classical Nucleation Theory and Atomic Scale Observations and Modeling *Advanced Engineering Materials* **8** 1231-1236

[13] Lépinoux J and Sigli C 2013 Precipitate growth in concentrated binary alloys: a comparison between kinetic Monte Carlo simulations, cluster dynamics and the classical theory *Phil. Mag.* **93** 3194-3215.

[14] Lépinoux J 2006 Contribution of matrix frustration to the free energy of cluster distributions in binary alloys *Phil. Mag.* **86** 5053–5082.
[15] Lépinoux J 2021 Modelling of the chemical potential in precipitation models *Phil. Mag.* **102** 95-111
[16] Lépinoux J and Sigli C 2019 Extracting free energy of clusters in concentrated binary alloys from atomistic Monte Carlo simulations *Modelling. Simul. Mater. Sci. Eng.* **27** 08500.
[17] Lépinoux J and Sigli C 2018 Multiscale modelling of precipitation in concentrated alloys: from atomistic Monte Carlo simulations to cluster dynamics: I. Thermodynamics *Phil. Mag.* **98** 1–19
[18] Lépinoux J 2020 Evolution of clusters free energy during precipitation in concentrated binary alloys *Phil. Mag. Letters* **100** 402-411.
[19] Lépinoux J 2021 What can we learn from the exclusion volume of fluctuations and precipitates? *Phil. Mag.* **101** 1097-111
[20] Voorhees P W 1985 The Theory of Ostwald Ripening *J. Of Statistical Physics* **38** 231-252
[21] Wang K G, Glicksman M E and Rajan K 2005 Length scales in phase coarsening: Theory, simulation, and experiment *Computational Materials Science* **34** 235–253
[22] Streitenberger P 2013 Analytical description of phase coarsening at high volume fractions *Acta Mater.* **61** 5026–5035
[23] Mahalingam K, Gu B P, Liedl G L and Sanders T H Jr 1987 Coarsening of δ´(Al3Li) precipitates in binary Al–Li alloys *Acta Metall.* **35** 483–98
[24] Robson J D 2004 Modelling the overlap of nucleation, growth and coarsening during precipitation *Acta Mater.* **52** 4669–76
[25] Perez M, Dumont M and Acevedo D 2008 Implementation of classical nucleation and growth theories for precipitation Acta Materialia 56 2119–2132